A method of calculating urban-scale solar potential by quantitating and evaluating the relationship between block typology and occlusion coefficient, a case study of a city in middle China

Abstract:

The existing macro-city-scale solar roof utilization potential assessment method is not capable of considering the factor of mutual occlusion between urban buildings, and only makes use to one empirical value for the entire urban rooftop potential calculation. Relevant research shows that under different occlusion conditions, the potential of solar energy utilization varies greatly. This paper selects urban blocks with different morphological characteristics as the research objects, and analyses and quantifies the influencing factors of solar potential of urban roofing. To measure the overall solar potential of the city, it is necessary to quantify the occlusion caused by the urban environmental building roof. The urban blocks in different types and functions of buildings have different occlusions on the building roof. To quantify these differences, this paper uses typical high-density blocks. Taking Wuhan as an example, a large number of urban block examples were selected as research samples, a large number of urban block form indicators were counted, and data sets covering six types of morphological indicators such as building density, building height, floor-area ratio and orientation were established. The difference between the morphological indicators of the block was used to classify the urban blocks, and then the solar radiation simulation of the above blocks was modelled and simulated. The solar radiation values of different blocks were obtained and combined with their morphological parameters. Linear regression was used to obtain different roof solar occlusion factors for different block types. They are 0.099, 0.054, and 0.025, and the overall roof occlusion coefficient of the city is 0.079.

Keywords:

Solar energy; Urban energy; Occlusion coefficient; K-means clustering algorithm

1. Introduction

1.1 Expansion of solar energy utilization to urban scale

The energy crisis and environmental pollution have always been major problems facing the world and are becoming increasingly serious. Urban energy consumption is an important part of global energy consumption evaluation. Related studies show that by 2030, 75% of energy consumption will come from cities (Cities and Climate Change, 2010). In order to meet people's growing demand for energy, renewable energy has become a hot topic for people to study. Compared with other renewable energy sources, such as wind energy and geothermal energy, solar energy is one of the few new energy sources that can be applied on a large scale in urban environments. The development and utilization of solar energy has received extensive attention and has been rapidly spread worldwide. Over the past decade, the global solar photovoltaic market has grown rapidly by 50%. The International Energy Agency (IEA) predicts that by 2050, the global share of electricity from photovoltaic (PV) systems will reach 16%. At present, the application of solar energy in single buildings has been relatively mature (Aaditya & Mani, 2017; *Technology Roadmap: Solar Photovoltaic Energy*, 2010). Based on this, research on solar energy utilization in urban environments has also begun to develop in a continuous and large-scale manner. At the same time, research on the potential of urban solar photovoltaic utilization in the world is quite extensive and has gradually moved towards applications. Therefore, it is of great scientific significance and application value to carry out research on the impact of urban-scale photovoltaic power generation utilization potential.

1.2 Existing problems in traditional methods of measuring solar photovoltaic utilisation potential

For the calculation of traditional solar photovoltaic potential, more software has been developed. Among these kinds of software, there is the Ladybug tool based on the Rhino and Grasshopper platform, and the CitySim software (D. Li et al., 2015; Ouria & Sevinc, 2018).

These kinds of software build the radiation model of the photovoltaic module (POA) by sunlight and accumulate the solar radiation over time to obtain the annual production capacity of the photovoltaic system. This type of method is called a method based on solar irradiance. However, for the calculation of solar energy potential at the city scale, the time-consuming accumulation method is too heavy and has little practical significance. For example, when determining the location of distributed solar energy in a city, methods at the city scale include the In My Backyard tool, the PVSITES project, and various GIS software-based methods (Anderson et al., 2010; Espeche et al., 2017). The PVSITES project is a large-scale photovoltaic installation and promotion project based on urban-scale solar potential distribution.

The estimation of urban-scale solar potential uses a top-down approach, which requires quantification of building roof area and urban environmental occlusion. Large-scale urban roof area information can be obtained using GIS data, neural network recognition methods for urban satellite images, and statistical methods for sampling estimation. A large number of studies have shown that neither the solar radiation distribution at the macro scale nor the quantification of roof area statistics is a problem (Araya-Muñoz et al., 2014; Bergamasco & Asinari, 2011; Kaynak et al., 2018; Y. Li et al., 2016; Wiginton et al., 2010). However, the quantification of urban environmental occlusion often lacks attention in the estimation of large-scale solar energy potential.

The quantification of the impact of dynamic shadow occlusion on solar energy between buildings is often not considered or only a unified empirical value is taken into consideration. The concept of occlusion and available roof area is used to introduce the concept of installation factors. Salvador Izquierdo et al. analyzed the roof installation factors of 17 types of buildings in Spain and found that the installation factor of roofs in Spain is about 0.78, but their research did not distinguish the types of buildings (Izquierdo et al., 2008); Luca

Bergamasco et al., in the photovoltaic utilization potential, classified the roof installation factors according to buildings, where the roof installation factors of residential and industrial plants were taken as 0.7 and 0.9, respectively (Bergamasco & Asinari, 2011). However, no systematic independent consideration of the impact of occlusion issues on solar potential has been accounted for. Considering that the city is a complex environment, the distribution of solar radiation affected by the occlusion problem is very uneven (Lobaccaro & Frontini, 2014), and the determination of the occlusion factor in the traditional method lacks a certain science. The dynamic shadow occlusion of the building surface has a great impact on solar energy utilization, which makes it difficult for the traditional large-scale quantification method of solar radiation on the building surface to treat streets with different occlusion conditions fairly, so it is difficult to play a role in actual planning and utilization.

1.3. Review of the research on the relationship between block morphology and block solar energy shielding

Occlusion is ignored because of the many influencing factors affecting the potential of solar photovoltaic utilization in cities. The environmental occlusion of a block is affected by the difference in weather conditions and the shape of the block, which is one of the most difficult factors to quantify. Among them, Taehoon Hong et al. studied the photovoltaic utilization potential of Gangnam District, Seoul, and estimated the photovoltaic utilization potential of the entire neighborhood. It was found that under the condition of real neighborhoods, the impact of blockages on photovoltaic utilization potential varies greatly. However, it is only described as an example (Hong et al., 2017). Kanters used the simulation software, Ecotect, to study the impact of urban density, land area, floor area ratio, and orientation on the use of shaded solar energy generated by the setting according to the two indicators of photovoltaic potential and power satisfaction rate. It is found that if the design is not reasonable, the solar

potential will decrease by 10% ~ 75% (Kanters, Wall, & Dubois, 2014; Kanters, Wall, & Kjellsson, 2014). These studies show that due to differences in climatic conditions, block shapes, density, and building spacing, the potential for solar energy caused by the mutual block between buildings in the blocks is significantly different. However, the occlusion of the block is not systematically analyzed according to the block type. Since the same types of city blocks have similar morphology, and the occlusion conditions caused by the morphology also have similarities, the typology classification of city blocks can be performed first, and the occlusion analysis for different types of blocks can be effective by simplifying calculations and making city data more accessible.

The clustering method is used to classify the blocks through the classification and calculation of the morphological parameters of different blocks in the city, and then carrying out a systematic research on each type of block, which can quickly and truly reflect the occlusion of the block in the city. Cluster analysis is an exploratory data analysis tool whose purpose is to organize a set of items (usually represented as a vector of quantitative values in a multidimensional space) into clusters to make the items in a given cluster highly similar (de Souza & de Carvalho, 2004), and belonging to different clusters has a high degree of similarity. In the study of urban air pollutants, Jing Zhang et al. used the K-means clustering algorithm to analyze the air pollutant types and proportion data, and obtained a cluster analysis of 74 cities in China (Zhang et al., 2016). Li Xinyi et al. combined the city's 2D satellite images and 3D building information and applied cluster analysis to the prototype classification of residential buildings to obtain the spatial distribution of different types of residential buildings in the city and the energy distribution characteristics of urban residential buildings (X. Li et al., 2018). The clustering method can classify a large amount of data with similarity and has high reliability.

It is necessary to quantify the occlusion impact according to the block type, and then quickly obtain the amount of solar radiation available on the building surface through the building surface area, and evaluate the power generation potential of distributed photovoltaic energy on urban buildings, which has an important role in improving energy efficiency and optimizing the energy structure of cities.

The purpose of this study is to solve the problem of mutual occlusion and neglect between the built environments in the calculation of urban-scale solar photovoltaic utilization potential. Based on the morphological characteristics of the city blocks, a clustering algorithm is used to classify them. The research can obtain the corresponding shielding coefficients and realize the problem of obtaining the spatial distribution characteristics of the solar photovoltaic utilization potential in the middle of the city through the shielding coefficients, and provide the basis for the overall solar building planning in the city.

2. Dataset and Methods

In this paper, the research on urban block occlusion is carried out in five steps **[Fig.1]**.

The first step is to obtain real block sample data. At this stage, field surveys, satellite maps, and street view pictures are used to obtain multidimensional parameters of city blocks, and a database is established based on various block morphological index types.

The second step is to classify the blocks. At this stage, the clustering algorithm is used to classify the blocks according to their morphological indicators, and the block types are analysed based on the classification results.

The third step is to calculate the solar radiation value of the above block. This step obtains data by using software simulation on the block model. The fourth step is to calculate and

analyse the average occlusion coefficient of different types of streets. This step uses a linear regression method.

The fifth step is to divide the shielding area of the central urban area of Wuhan according to the calculation results of Part 4, and modify the solar radiation potential value.

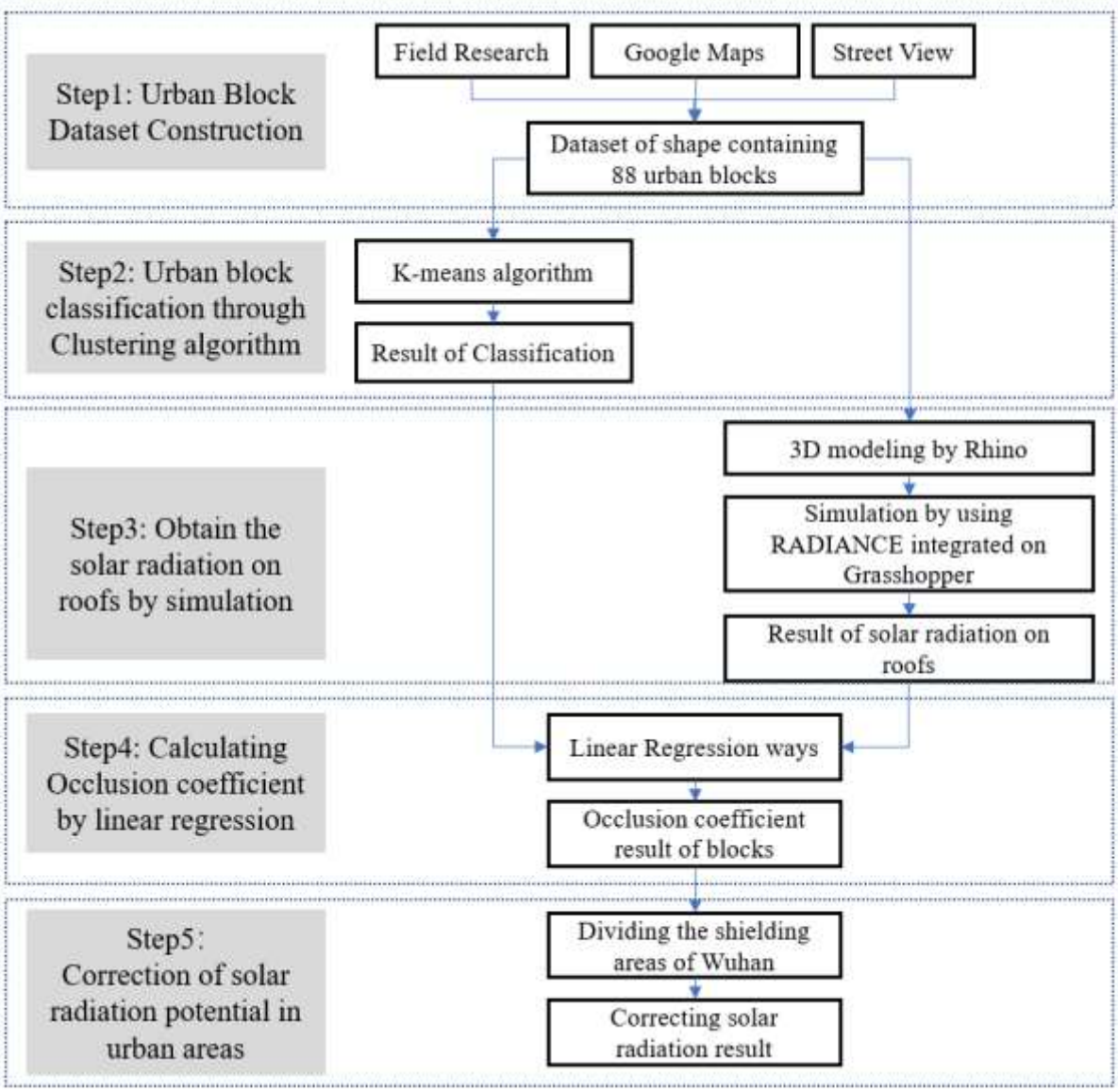

Fig.1 Schematic of the analysis workflow.

2.1 Acquisition of real block sample data

2.1.1 Urban block data

In this paper, within 88 selected districts with different morphological characteristics in Wuhan's electoral districts, the actual measurement and 3D buildings are used to obtain the real urban block. The case is to provide a data set for studying the urban roofing occlusion coefficient through research on representative cases. Therefore, the selection of urban block examples in this study follows three principles:

- Satisfy the diversity of block layout morphological characteristics: The diversity of block morphological characteristics includes the diversity of planar layout patterns and the diversity of height layout patterns. The selection on the diversity of the planar layout form includes determinants, courtyards, dislocations, etc. The diversity of the height layout form includes the bottom, multilayer, high-rise, and high-low staggered layout of urban blocks.

- Satisfy the diversity of urban area distribution: The selected urban blocks cover the central area of the city to the periphery of the city. The difference in urban spatial form caused by this urban area distribution is often reflected in the building density, such as the high density of the city centre, and low density in the suburbs.

- Satisfy the diversity of the architectural functions of the block: The function of a specific city block often determines the shape of the city block. This article covers the selection of city block cases, covering different types of functions such as industrial blocks, commercial blocks, residential blocks, schools, and institutions.

2.1.2 Classification indicators of urban blocks

In previous studies, the influencing factors that control the type characteristics of the block are: Site Area(SA), Gross Floor Area(GFA), Building Volume(BV), Building Footprint Area(BFA), Envelope Surface Area(ESA), Building Perimeter(BP), Number of Buildings, Building Orientation, Building Height(BH), Building Density(BD), BSA/BV, BP/BFA.

Comprehensively considering the land use indicators considered in the relevant literature and whether they are easy to obtain (Dekay & Brown, 2001; Montavon, 2010; Wei et al., 2015), this study considers the impact of 5 morphological index factors on the statistics of 88 block samples:

• Building height (BH): the vertical distance from the building roof to the ground. For the block, this study counts the average building height of the buildings in the block;

• Building density (BD): the ratio of the projected area of the building to the total area of the block;

• Building Surface area/Building Volume (BSA/BV): the ratio of the building's external surface area to the building's volume;

• Building Perimeter/ Building Footprint Area (BP/BFA): the ratio of the total length of the building's outer contour to the building's floor area;

• Floor area ratio (FAR): the ratio of the total area of all floors of a building to the total area of the block.

In this paper, a large number of blocks with different morphological characteristics are selected as samples in typical cities for actual measurement and 3D modelling, and a data set is established. [A1]

2.2 Calculation method of solar radiation based on simulation

Traditionally, the radiation measurement method is to obtain the total radiation sensor. However, it is difficult to install sensors on a large scale on real urban street roofs. Simultaneously, the actual measurement methods are difficult to carry out on a large scale. Therefore, it is necessary to use simulation methods to measure the radiation in the real environment. For the calculation of solar radiation on roofs in urban blocks, the key to simulation is the setting of boundary parameters and whether the parameters are suitable for the urban and meteorological environment of the study area. Therefore, the accuracy of the simulation software needs to be verified.

Urban block solar simulation has three parts: urban block 3D modelling tool, solar simulation tool and simulation results visualization tool. In this study, the 3D model of the urban block model used was on Rhinoceros 6.0, and the solar simulation tool selected was the Radiance radiation simulation software which is widely used. This software uses the Perez diffusion radiation model (Perez et al., 1987, 1990) and has had many successful applications (Jakubiec & Reinhart, 2013; Reinhart & Walkenhorst, 2001). Integrated into Rhinoceros 6.0, the Ladybug & Honeybee plug-in of the Grasshopper visual programming platform built in Rhinoceros 6.0 is used for the operation and visualization of measurement results.

2.3 Clustering algorithm

In this study, the K-means algorithm was used to perform a cluster analysis on five types of morphological data and radiation per unit area of building roofs in 88 blocks, and the block samples were divided into three block types.

Cluster analysis refers to the classification of samples based on individual characteristics, so individuals in the same category will have a high degree of homogeneity, while individuals in

different categories will have a high degree of heterogeneity. Through this method, multiple classification of indicators, and the classification characteristics of samples can be expressed intuitively.

The Fig.2 shows the code implementation of the K-means algorithm used in this study.

File Edit View Insert Cell Kernel Widgets Help

运行 代码

In [18]:

```
def kmeans(k, epsilon=0, distance='euclidian'):
    history_centroids = []
    if distance == 'euclidian':
        dist_method = euclidian
    dataset = load_dataset('durudataset.txt')
    # dataset = dataset[:, 0:dataset.shape[1] - 1]
    num_instances, num_features = dataset.shape
    prototypes = dataset[np.random.randint(0, num_instances - 1, size=k)]
    history_centroids.append(prototypes)
    prototypes_old = np.zeros(prototypes.shape)
    belongs_to = np.zeros((num_instances, 1))
    norm = dist_method(prototypes, prototypes_old)
    iteration = 0
    while norm > epsilon:
        iteration += 1
        norm = dist_method(prototypes, prototypes_old)
        prototypes_old = prototypes
        for index_instance, instance in enumerate(dataset):
            dist_vec = np.zeros((k, 1))
            for index_prototype, prototype in enumerate(prototypes):
                dist_vec[index_prototype] = dist_method(prototype,
                                                        instance)

            belongs_to[index_instance, 0] = np.argmin(dist_vec)

        tmp_prototypes = np.zeros((k, num_features))

        for index in range(len(prototypes)):
            instances_close = [i for i in range(len(belongs_to)) if belongs_to[i] == index]
            prototype = np.mean(dataset[instances_close], axis=0)
            # prototype = dataset[np.random.randint(0, num_instances, size=1)[0]]
            tmp_prototypes[index, :] = prototype

        prototypes = tmp_prototypes

        history_centroids.append(tmp_prototypes)

    # plot(dataset, history_centroids, belongs_to)

    return prototypes, history_centroids, belongs_to
```

Fig.2 Clustering Algorithm Code

2.4 Calculation method of solar occlusion coefficient

The total solar roof radiation in urban blocks is positively related to the building roof area in urban blocks. Therefore, a linear regression algorithm can be used to obtain a linear regression model of solar roof radiation in urban blocks. Since different types of streets have

different occlusions on the roof, the difference reflected in the linear regression model is the slope of the regression curve. Therefore, the slope of the regression curve can be used to calculate the solar occlusion coefficient of urban roofs.

A commonly used method for calculating solar radiation uses the three factors that affect the solar radiation on the roof to multiply by linear correlation. The calculation formula is as follows:

$$R_{Total} = S_{roof} \times R_{Unit} \times (1 - \eta_{OF})$$

In this formula, R_{Total} is the available solar radiation on the roof of the block; S_{roof} is the available solar roof area on the block; R_{Unit} is the amount of solar radiation per unit area under unblocking conditions; η_{OF} is the block coefficient of the block, where the block coefficient η_{OF} is a measure of the coefficient of urban block environment on the occlusion of a building roof. The value ranges from 0 to 1, where the larger the value, the more severe the occlusion of the roof in this area.

In this study, in order to determine the occlusion coefficient value η_{OF} under different street types, a linear regression method was used. By performing linear regression on the R_{Total} and S_{roof} values of the block samples, the occlusion coefficient η_{OF} of the block is calculated. The specific calculation formula is as follows:

$$\eta_{OF} = 1 - B/B_{Origin}$$

In the formula, η_{OF} is the occlusion coefficient of the street, B is the slope of the curve after linear regression analysis, and B_{Origin} is the slope value of the curve under the condition of no occlusion, which is equivalent to R_{Unit} in value.

By analysing different block types, the occlusion coefficient η_{OF} of different block types can be obtained, and the regression analysis of all samples is capable of obtaining the average occlusion coefficient of the entire city.

3. Results

3.1 City block classification based on clustering algorithm

In this study, the Python scripting language was used to implement the clustering algorithm in the Jupyter Notebook development environment. After the 88 city block samples were classified according to the characteristics of the five indicators, three different differences in the urban form indicators were obtained. Clustering algorithm data results and visual classification results are shown in Fig.3 and Fig.4.

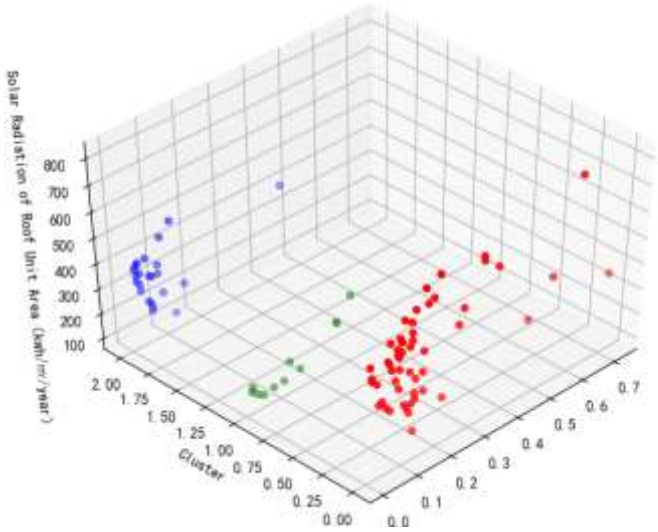

Fig.3 Cluster Results Visualization

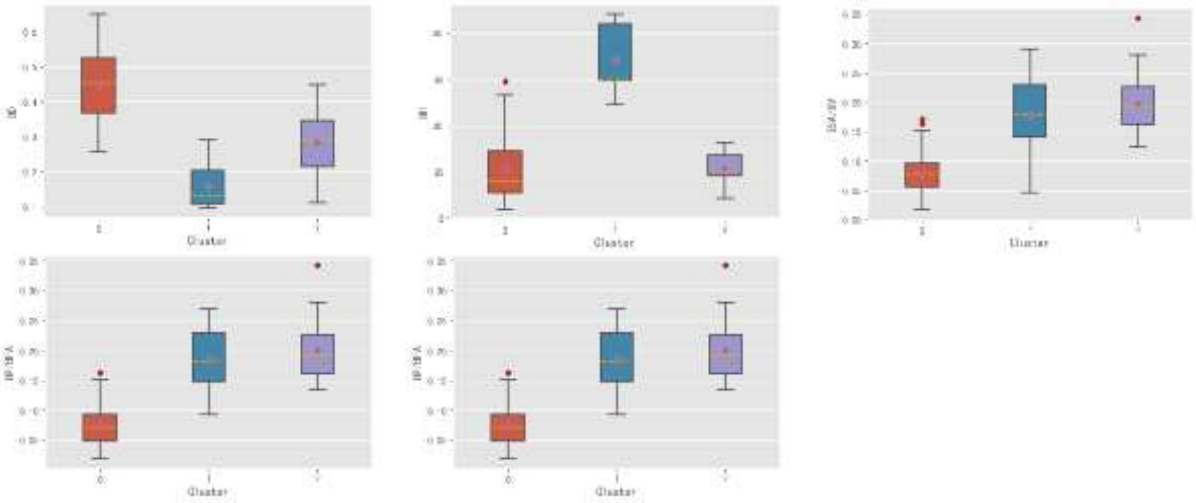

Fig.4 Cluster Algorithm Classification Result Indicator Distribution Characteristics

According to the classification results of the clustering algorithm, 88 urban block samples are divided into 3 different types. By analysing the corresponding indicators of these three categories, the corresponding three types of urban blocks are summarized (**Table 2**). The characteristics are as follows:

Table 2
Cluster Algorithm Classification Result Statistics

Cluster Type	BH	BD	ESA/BV	BP/BFA	FAR
Cluster 0	Low & Middle	High	Low	Low	Middle
Cluster 1	High	Low	Middle	Middle	High
Cluster 2	Low	Middle	High	High	Low

Cluster0: low-rise or middle-rise, high-density blocks, represented by industrial plants and middle-high rise residential areas(24M<BH<60M);

Cluster 1: high-rise, low-density block, represented by commercial complexes and office buildings;

Cluster 2: Low-rise, medium-density block, represented by multi-storey residential areas (BH<24M).

3.2 Calculation of solar energy utilization potential occlusion coefficient in different types of blocks

Since different types of urban blocks have different potentials for solar energy utilization, after classification of urban blocks, three different types have been obtained. This section separately measures the amount of solar radiation from the roof of these three types of urban blocks, using linear regression. The method obtains the roof solar radiation regression model of the corresponding type of urban block, and finally calculates the roof solar occlusion coefficient of the type of block.

3.2.1 Linear regression analysis verification

Through linear simulation of roof solar energy in 88 real urban blocks, and linear regression calculation of solar radiation amount and block building density of roof unit area, linear regression analysis was carried out for three different types of urban blocks, and the overall

linear regression analysis was carried out in 88 urban blocks. The overall regression curves and correlation coefficients of the three types of blocks and urban blocks were obtained as follows (**Fig.5, Table 3**).

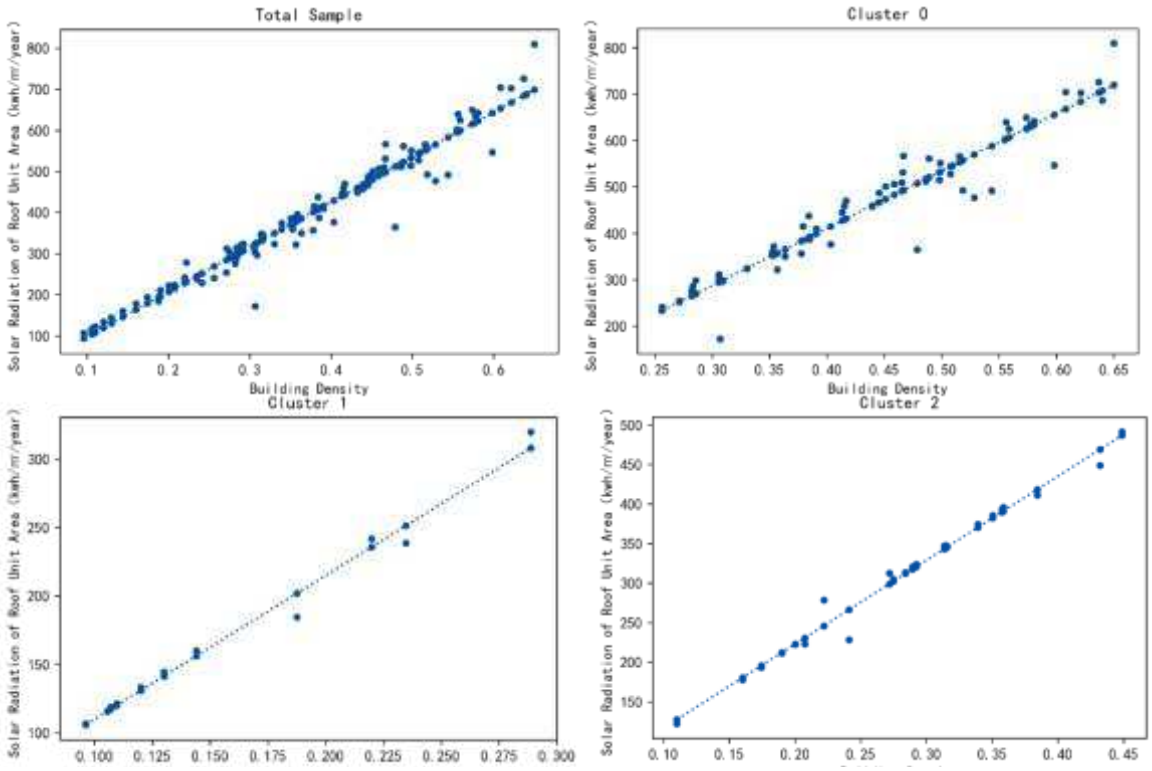

Fig.5 Linear Regression Curve

Table 3
Regression Curve and Correlation Coefficient Statistics

Type	Curve Slope	R^2
Cluster 0	1235.8	0.8997
Cluster 1	1049.2	0.9856
Cluster 2	1061.2	0.9822
Total	1093.7	0.9437

The study found that in the three types of urban blocks, because the degree of occlusion of different types of urban block roofs is different, the slope of the regression curve is different, and the correlation R2 of the regression curve is about 0.9, so It is proved that the general linear model is applicable to the regression analysis of solar radiation quantity and building density of the roof unit area.

3.2.2 Estimation of occlusion coefficient

The solar occlusion coefficient is calculated by calculating the solar opacity coefficient of the radiation amount and the building density regression curve of the roof unit area of three different types of blocks and sample populations (**Table 4**). It is found that the difference of roof solar occlusion coefficient of different types of blocks is obvious, for cluster 1, 2, and 3, the roof solar occlusion coefficient averages are 0.099, 0.054, 0.025 for the city's overall 88 urban block samples, the calculated roof solar occlusion coefficient average is 0.079, that is, the city's overall average. The roof will obstruct 8% of the solar energy, and the remaining 92% of the solar energy will be used by roofing solar installations.

Table 4

Occlusion Coefficient with Block Type

Cluster Type	Feature	Curve Slope	Occlusion Coefficient	Block Type
Cluster 0	Middle and Low Rise; High Density	1235.8	0.099	Industrial Block; Middle-High rise reidential Areas
Cluster 1	High Rise; Low Density	1049.2	0.054	Commercial Complexes; Office Builidings
Cluster 2	Low Rise; Middle Density	1061.2	0.025	Multi-storey Residential Areas
Total	-	1093.7	0.079	-

For the cluster 0 block, that is, the middle and low-rise high-density blocks represented by industrial plants and middle-high rise residential areas(24M<BH<60M), the average occlusion coefficient is 0.099;

For the cluster 1 block, that is, the high-rise low density represented by commercial complexes and office buildings, the average occlusion coefficient is 0.054;

For the cluster 2 block, that is, a low-density medium-density block represented by multi-storey residential areas (BH<24M), the average occlusion coefficient is 0.025; (**Fig.6**)

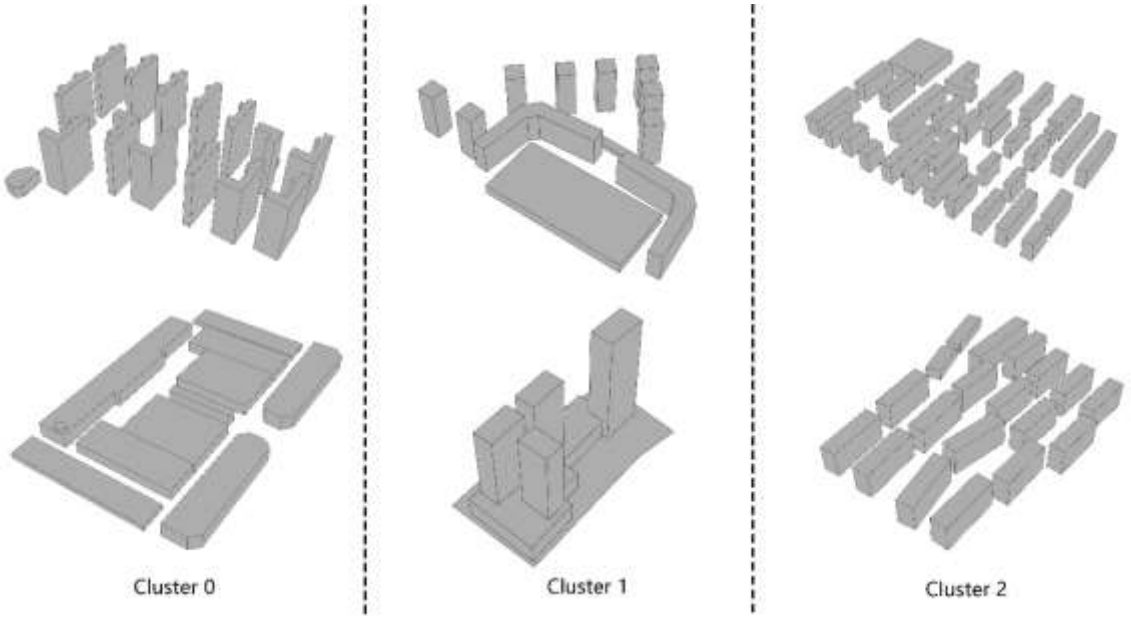

Fig.6 Block Type Models of Clustering Results

In summary, the occlusion coefficient of the three types of blocks is less discrete, so when calculating the solar energy application potential of the corresponding block, the average value of the corresponding occlusion coefficient can be used for calculation.

For the city as a whole, the overall occlusion coefficient is close to the average level of 0.079, but in the city scale measurement, when the roof occlusion coefficient needs to be simplified, the value can be used to simplify the calculation.

3.3 Calculate solar energy utilization potential at macro city scale based on occlusion coefficient

3.3.1 Using open source channels to obtain the roof area of Hongshan District in Wuhan City

Taking Hongshan District in Wuhan as an example, this paper estimates the potential of photovoltaic utilization in Hongshan District. The study area and recognition result are shown in Fig.7 and Fig.8

Fig.7 The Range of Hongshan District

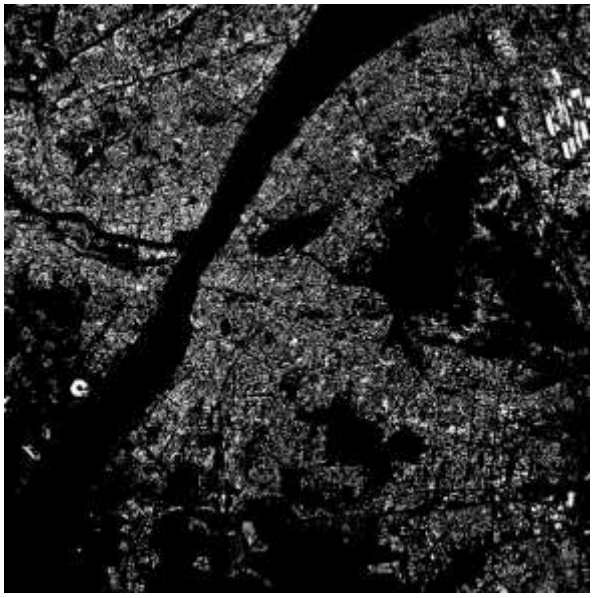

Fig.8 Recognition Result of Study Area

329

330 The red line is the range of Hongshan District in Wuhan, which is defined by the Wuhan City
331 Master Plan (2006-2020)(Wuhan Natural Resources and Planning Bureau, 2011). The urban
332 area of Hongshan District is 480 square kilometres. Using the open source Wuhan GIS map
333 file to calculate the roof area of Hongshan District, the total available roof area of Hongshan
334 District is 41380900 m^2.

335 ***3.3.2 Blocking the urban area of Hongshan District based on the obtained occlusion***
336 ***coefficient***

337 Then the measured corresponding type roof occlusion coefficient was used to simplify the
338 calculation of the overall occlusion of the city.

339 In the urban three-dimensional GIS file for different plots of the city, they were classified into
340 different types of occlusion coefficients, and were assigned to different occlusion coefficients
341 in calculating the overall solar photovoltaic utilization potential of the urban scale as shown in
342 **Fig.9**.

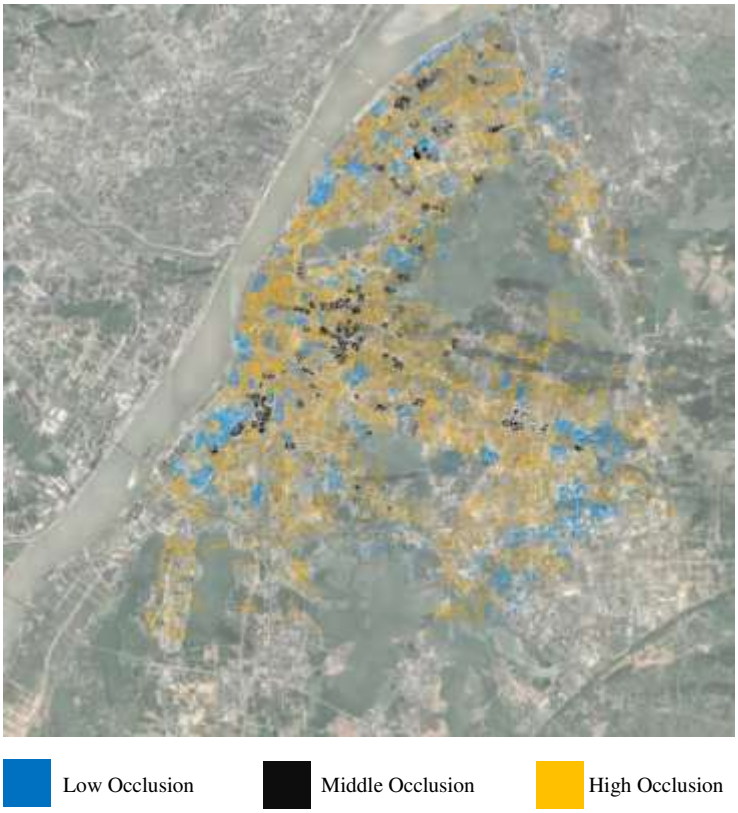

Fig.9 Occlusion Coefficient Visualization

Blue represents low occlusion (0.025), i.e. the cluster 2 block, whilst black represents medium occlusion (0.054), i.e. the cluster 1 block, and orange represents severe occlusion (0.099), i.e. the cluster 0 block, where the overall occlusion coefficient is 0.079. but in the city scale measurement, when the roof occlusion coefficient needs to be simplified, the value can be used to simplify the calculation.

3.3.3 Correcting the urban solar radiation according to the occlusion coefficient

In this section, in the setting of the calculation parameters, the annual radiation per unit area of Hongshan District is 1150 kWh/m2/year. After correcting, the total roof solar radiation in Hongshan District is 45208.30 GWh/year.

4. Applicable analysis and Theory

4.1. Occlusion coefficient applicability verification

This study is based on the study of solar occlusion coefficient in real city blocks in Wuhan. It measures the solar occlusion coefficient of urban roofs for different types of blocks and cities. However, whether the roof occlusion coefficient measured in the urban environment of Wuhan is applicable to the whole world needs to be verified and analysed.

In terms of differences in urban meteorological conditions, the factors affecting the urban roof occlusion coefficient are mainly the solar elevation angle, that is, the solar elevation angle decreases with increasing latitude, and the roof solar occlusion coefficient decreases under the same urban form, in order to verify the urban roof due to differences in urban meteorological conditions. The influence of the solar occlusion coefficient is verified by the solar radiation simulation method in 11 major cities in the world. The verification model is selected from a typical urban block belongs to cluster 2 in Wuhan and is carried out under different meteorological conditions. The roof solar radiation simulation simulates and measures the roof solar occlusion coefficient. (Table 5)

Table 5

Occlusion Coefficient Verifying Result Of 11 Main City in The World

Number	City Name	Latitude	Case Block Occlusion Number
1	Singapore	1.3	0.018073705
2	Bangkok	13.4	0.018194903
3	Mumbai	18.5	0.023502853
4	Beijing	39.9	0.045298833
5	Cairo	30	0.029726544
6	Shanghai	31.1	0.03294302
7	New York	40.4	0.037121775
8	Paris	48.5	0.037112789
9	London	51.3	0.044234758
10	Sydney	-33.8	0.014304145
11	Rio de Janeiro	-22.5	0.01363006

In this study, the occlusion coefficient is calculated for 11 major cities in different latitudes in the world (Fig.10). The calculated R-squared value is 0.8673, which indicates that in different latitude urban environments, it can be considered that the roof solar occlusion coefficient is linearly positively correlated by meteorological conditions. According to the calculation, in the same city form, the roof solar occlusion in the northern area will be higher than that in the south. The relationship between the meteorological and occlusion coefficients makes it possible to calculate other urban occlusions according to the Wuhan occlusion coefficient

.

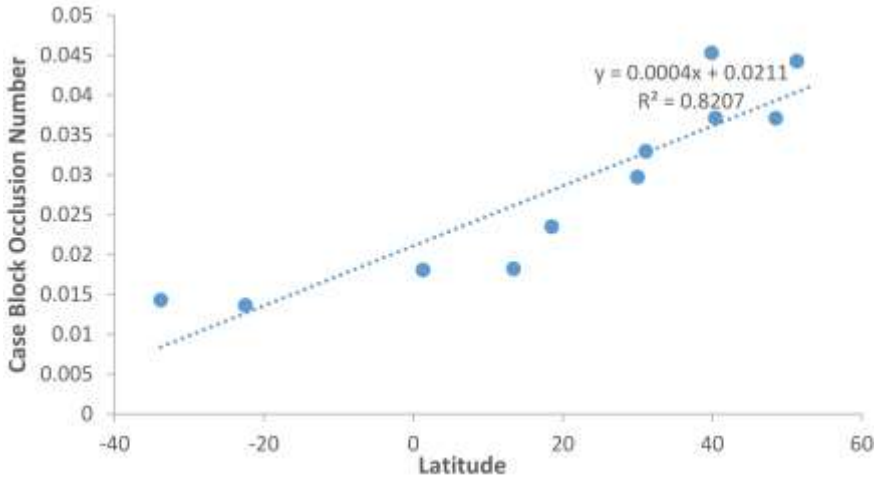

Fig.10 Linear Regression Curve

4.2 Conclusion

This paper proposes a method to quantify the problem of block occlusion in the use of solar energy. Then take Wuhan City as an example to use the obtained occlusion coefficient type to classify the relevant urban roofs and calculate the total solar energy potential of the city. Compared with occlusion, the city will produce 7% error, especially in the low-rise high-density block or the high-rise office block occlusion coefficient will cause 10% error.

In typical high-density cities, urban block types have commonalities, so the occlusion coefficients of different types of blocks proposed in this paper have certain applicability. There are differences in the

387 solar occlusion coefficients of different types of blocks. They are weak occlusion (0.01 occlusion
388 coefficient) represented by industrial type blocks, middle occlusion (blocking coefficient 0.04)
389 represented by middle and high-rise residential areas, and high occlusion represented by commercial
390 type blocks (the occlusion factor is 0.13).

391 As far as the city as a whole is concerned, the urban block environment has different influences on the
392 roofing of the city depending on the block. In different cities around the world, the roof solar occlusion
393 coefficient is linearly positively correlated with the climatic conditions. The roof occlusion coefficient
394 in Wuhan can be that it provides reference for the calculation of roof solar energy utilization in other
395 cities around the world. This paper calculates in Wuhan area and provides reference for occlusion
396 coefficient for solar energy measurement in other high-density cities.

397

Appendices:

A1

88 Block Morphology Parameters

Number	Site Area(SA)	Gross Floor Area (GFA)	Building Volume(BV)	Building Footprint Area(BFA)	Envelope Surface Area(ESA)	Building Perimeter(BP)	Number of Buildings	Orientation	Building Height(BH)	Building Density(BD)
1	38588.00	69847.00	907978.90	11941.00	35389.00	828.78	6	3	42.90	0.31
2	28293.00	91222.00	401033.68	12588.00	69855.00	1119.65	3	3	31.86	0.44
3	11423.00	40176.00	133078.40	6192.00	25770.00	659.47	3	2	32.70	0.27
4	90700.00	127082.00	533844.70	34833.00	41275.00	2857.00	12	2	15.90	0.38
5	66268.00	89445.00	424528.00	25120.00	30658.00	2316.00	9	2	16.90	0.42
6	33881.00	43866.00	138561.00	7544.00	31437.00	1717.00	20	4	18.50	0.22
7	187984.00	175834.00	1256400.00	43766.00	35389.00	6026.00	31	2	15.00	0.65
8	579373.00	360989.00	4367422.45	322319.00	71938.00	6860.00	12	2	13.55	0.56
9	129413.00	78111.00	580779.00	64531.00	50177.00	3653.00	31	3	9.00	0.50
10	106181.00	54436.00	339025.91	51000.00	24855.00	5102.00	25	4	6.99	0.49
11	45797.00	22262.00	100179.00	22262.00	8053.00	1798.00	6	3	4.50	0.49
12	52790.00	33984.00	221048.00	24560.00	22478.00	2514.00	12	6	9.00	0.47
13	168734.00	127180.00	895824.00	86078.00	45253.00	5586.00	17	3	8.00	0.52
14	87182.00	59822.00	386053.60	34034.00	31443.00	3402.00	11	3	8.40	0.39
15	45774.00	124425.00	353367.00	24885.00	42279.00	3020.00	15	4	14.20	0.54
16	34251.00	46116.00	129124.80	15372.00	22680.00	2700.00	18	6	8.40	0.45
17	238787.00	256209.00	721704.20	107726.00	68380.00	6519.00	34	1	6.70	0.45
18	228974.00	296531.50	1189387.50	80925.00	142518.00	8740.00	57	4	14.70	0.35
19	212311.00	101902.00	1096305.92	99082.00	40388.00	3462.00	10	3	10.56	0.47
20	223372.00	155379.00	1522480.40	104271.00	93262.00	7039.00	28	2	14.60	0.47
21	179978.00	103336.00	1238832.00	103336.00	29928.00	2494.00	3	4	12.00	0.57
22	202857.00	91825.00	1003643.40	76614.00	46283.00	3698.00	13	2	13.10	0.38
23	103770.00	71796.00	644826.00	61412.00	35536.00	3198.00	11	3	10.50	0.58
24	46742.00	39876.00	389013.40	28118.00	20126.00	2368.00	12	6	10.30	0.56
25	54359.00	35112.00	358968.80	24027.00	15412.00	1162.00	4	6	14.40	0.46
26	96803.00	79400.00	698320.00	60200.00	32965.00	2804.00	8	6	11.60	0.62
27	30133.00	21283.00	192476.40	20049.00	11315.00	990.80	3	6	9.60	0.66
28	28577.00	17267.00	138603.90	14551.00	15121.00	1220.00	7	3	10.90	0.51
29	27138.00	17276.00	207312.00	17276.00	10833.00	902.00	2	6	12.00	0.64
30	656801.00	399469.00	4436888.40	399469.00	234129.00	63638.00	45	4	3.60	0.61
31	349788.00	223828.00	805780.80	223828.00	121826.00	33840.00	23	1	3.60	0.64
32	93948.70	183211.62	732845.69	12214.00	134761.54	2240.00	11	4	60.00	0.13
33	51693.89	45048.78	180195.13	9009.76	40322.39	3936.00	13	3	20.00	0.17
34	48048.42	53869.06	215476.25	7695.58	41490.79	1481.00	9	3	28.00	0.16
35	27300.75	22555.19	90220.77	7518.40	19257.78	1604.00	13	2	12.00	0.27
36	24084.67	33795.01	135180.04	6827.98	27820.78	1350.00	10	4	28.00	0.28
37	20639.66	54634.00	212491.67	10624.60	50999.23	2484.00	27	4	20.00	0.36
38	98074.86	141556.00	566227.58	9437.13	101986.90	1600.00	9	2	60.00	0.10
39	46912.31	44012.00	176259.32	13712.18	30694.06	2859.00	19	2	13.00	0.29
40	99088.80	159269.00	625867.44	31250.37	144579.40	7096.00	65	3	20.00	0.32
41	80664.39	186793.00	726810.93	8863.55	136880.15	1570.00	14	5	82.00	0.11
42	71873.95	130899.00	554303.82	25195.63	106812.37	4833.00	41	3	22.00	0.35
43	44931.46	79238.00	289529.34	15238.39	54349.45	2673.00	16	3	19.00	0.34
44	111300.31	240578.21	982312.84	16038.55	154099.15	2567.00	15	3	60.00	0.14
45	38817.19	69932.00	249819.18	13878.34	54470.34	2885.00	33	3	18.00	0.36
46	62716.36	100274.00	744716.28	13791.04	215899.23	3718.00	26	4	34.00	0.22
47	83175.37	219638.65	878554.59	9983.57	216282.54	2457.00	15	3	88.00	0.12
48	87045.14	131611.00	497592.83	18058.99	81613.33	2794.00	22	3	27.00	0.21
49	62470.85	121188.00	1613141.22	18331.15	75980.01	2457.00	15	3	88.00	0.29
50	176900.47	276388.00	1111386.42	18827.06	265817.27	4492.00	27	4	59.00	0.11
51	113959.06	189021.00	981779.97	36362.22	126009.67	5758.00	40	4	27.00	0.31
52	47706.69	88505.00	187001.23	18233.65	64135.55	6270.00	72	2	10.20	0.38
53	76324.04	100272.00	398789.95	14499.67	93863.54	3394.00	32	4	27.50	0.19
54	125871.92	93297.00	370298.00	13866.67	69342.26	2448.00	19	3	26.70	0.11
55	103243.87	196652.00	823699.96	29878.91	121743.48	4484.00	31	3	27.50	0.29
56	58521.53	89365.00	353773.57	18425.71	55697.24	2879.00	20	2	19.20	0.31
57	162953.68	354824.00	1470388.93	17197.53	321516.23	5777.00	30	3	85.50	0.11
58	143202.94	228119.00	1101426.51	41251.93	144748.73	6771.00	41	4	26.70	0.28
59	78991.06	282930.00	1131720.00	42394.00	51222.00	796.31	1	0	27.00	0.60
60	6230.58	12412.00	49648.00	3103.00	4464.00	249.10	1	5	16.00	0.50
61	22716.55	34365.00	137460.00	11455.00	16791.00	1664.13	7	1	12.00	0.41
62	47574.74	198746.00	794984.00	24663.00	39007.00	614.86	1	0	32.00	0.52
63	69773.74	322329.00	1289280.00	40290.00	53404.00	2822.41	8	2	32.00	0.58
64	27383.43	192029.00	768116.00	12109.00	71939.00	1501.81	1	4	59.00	0.68
65	100740.87	306960.00	1227840.00	51160.00	73947.00	1501.81	5	1	29.00	0.51
66	81656.92	289211.00	1156844.00	31452.00	72899.00	1168.37	4	0	37.00	0.39
67	19191.03	18540.00	72560.00	6839.00	72570.00	994.60	3	0	11.00	0.36
68	18908.81	100997.00	403988.00	9991.00	31600.00	494.32	1	2	41.00	0.53
69	82440.95	239477.00	957909.00	34211.00	39463.00	1364.26	3	3	28.00	0.41
70	41844.37	217427.00	869708.00	31061.00	16307.00	723.52	1	3	28.00	0.65
71	42193.45	197388.00	789472.00	14874.00	62608.00	973.45	2	2	53.00	0.33
72	55918.51	167033.00	668132.00	17106.00	71326.00	1253.74	7	0	39.00	0.31
73	13558.80	23432.00	93728.00	3858.00	14868.00	1241.99	6	2	16.00	0.43
74	85538.39	158412.00	633648.00	25509.60	47706.24	1455.85	3	3	35.00	0.31
75	98439.47	254721.00	1019884.00	29796.79	72261.32	2104.01	5	3	34.00	0.31
76	94214.99	221969.00	887876.00	34233.53	69908.94	2565.42	5	2	26.00	0.36
77	68585.64	260171.00	1040684.00	16099.62	90846.12	1481.57	4	2	65.00	0.23
78	44300.17	81546.00	326184.00	12539.74	38238.31	1319.49	4	0	26.00	0.28
79	72875.03	167413.00	669652.00	13671.47	61367.22	1629.28	7	4	49.00	0.19
80	78691.51	275515.00	1102060.00	31043.66	83780.68	2055.02	4	2	35.00	0.40
81	110413.53	287803.00	1151220.00	41853.92	68509.23	2265.80	2	6	27.00	0.38
82	78117.59	213557.00	854228.00	20005.61	67361.39	2006.44	3	0	43.00	0.26
83	68085.17	99610.00	398440.00	19209.44	60669.97	1958.62	3	6	21.00	0.28
84	131121.03	234904.00	939616.00	43203.13	53684.79	2209.71	2	0	22.00	0.33
85	109408.11	169873.00	759492.00	29065.16	62733.88	2143.48	12	2	26.00	0.27
86	68062.94	116000.00	867600.00	16421.23	63811.70	2208.94	9	0	28.00	0.24
87	218700.83	367373.00	2269492.00	62451.49	109448.18	3301.32	12	2	36.00	0.29
88	158403.84	349557.00	1398228.00	49589.26	78941.63	2051.87	3	4	29.00	0.44

Funding:

This research was supported by the National Natural Science Foundation (No. 51678261), State Key Laboratory of Subtropical Building Science (No. 2017ZB08), and Wuhan Urban, Rural Construction Committee (No. 201726) and Fundamental Research Funds for the Central Universities (No.2019kfyXKJC029).

References

Aaditya, G., & Mani, M. (2017). Integration of Photovoltaics in Buildings. In *Encyclopedia of Sustainable Technologies* (pp. 259–273). https://doi.org/10.1016/B978-0-12-409548-9.10201-5

Anderson, K. H., Coddington, M. H., & Kroposki, B. D. (2010). Assessing technical potential for city PV deployment using NREL's in my backyard tool. *2010 35th IEEE Photovoltaic Specialists Conference*, 001085–001090. https://doi.org/10.1109/PVSC.2010.5614697

Araya-Muñoz, D., Carvajal, D., Sáez-Carreño, A., Bensaid, S., & Soto-Márquez, E. (2014). Assessing the solar potential of roofs in Valparaíso (Chile). *Energy and Buildings*, *69*, 62–73. https://doi.org/10.1016/j.enbuild.2013.10.014

Bergamasco, L., & Asinari, P. (2011). Scalable methodology for the photovoltaic solar energy potential assessment based on available roof surface area: Application to Piedmont Region (Italy). *Solar Energy*, *85*(5), 1041–1055. https://doi.org/10.1016/j.solener.2011.02.022

Brentan, B., Meirelles, G., Luvizotto, E., & Izquierdo, J. (2018). Hybrid SOM+ k -Means clustering to improve planning, operation and management in water distribution systems. *Environmental Modelling & Software*, *106*, 77–88. https://doi.org/10.1016/j.envsoft.2018.02.013

Cities and Climate Change. (2010). OECD. https://doi.org/10.1787/9789264091375-en

de Souza, R. M. C. R., & de Carvalho, F. de A. T. (2004). Clustering of interval data based on city–block distances. *Pattern Recognition Letters*, *25*(3), 353–365. https://doi.org/10.1016/j.patrec.2003.10.016

Dekay, M., & Brown, G. Z. (2001). SUN, WIND & LIGHT: Architectural Design Strategies. In *Society of Building Science Educators*. John Wiley and Sons Inc.

Espeche, J. M., Noris, F., Lennard, Z., Challet, S., & Machado, M. (2017). PVSITES: Building-Integrated Photovoltaic Technologies and Systems for Large-Scale Market Deployment. *Proceedings*, *1*(7), 690. https://doi.org/10.3390/proceedings1070690

Hong, T., Lee, M., Koo, C., Jeong, K., & Kim, J. (2017). Development of a method for estimating the rooftop solar photovoltaic (PV) potential by analyzing the available rooftop area using Hillshade analysis. *Applied Energy*, *194*, 320–332. https://doi.org/10.1016/j.apenergy.2016.07.001

Izquierdo, S., Rodrigues, M., & Fueyo, N. (2008). A method for estimating the geographical distribution of the available roof surface area for large-scale photovoltaic energy-potential evaluations. *Solar Energy*, *82*(10), 929–939. https://doi.org/10.1016/j.solener.2008.03.007

Jakubiec, J. A., & Reinhart, C. F. (2013). A method for predicting city-wide electricity gains from photovoltaic panels based on LiDAR and GIS data combined with hourly Daysim simulations. *Solar Energy*, *93*, 127–143. https://doi.org/10.1016/j.solener.2013.03.022

Kanters, J., Wall, M., & Dubois, M.-C. (2014). Typical Values for Active Solar Energy in Urban Planning. *Energy Procedia*, *48*, 1607–1616. https://doi.org/10.1016/j.egypro.2014.02.181

Kanters, J., Wall, M., & Kjellsson, E. (2014). The Solar Map as a Knowledge Base for Solar Energy Use. *Energy Procedia*, *48*, 1597–1606. https://doi.org/10.1016/j.egypro.2014.02.180

Kaynak, S., Kaynak, B., & Özmen, A. (2018). A software tool development study for solar energy potential analysis. *Energy and Buildings*, *162*, 134–143. https://doi.org/10.1016/j.enbuild.2017.12.033

Lee, D., & Oh, K. (2018). Classifying urban climate zones (UCZs) based on statistical analyses. *Urban Climate*, *24*, 503–516. https://doi.org/10.1016/j.uclim.2017.06.005

Li, D., Liu, G., & Liao, S. (2015). Solar potential in urban residential buildings. *Solar Energy*, *111*, 225–235. https://doi.org/10.1016/j.solener.2014.10.045

Li, X., Yao, R., Liu, M., Costanzo, V., Yu, W., Wang, W., Short, A., & Li, B. (2018). Developing urban residential reference buildings using clustering analysis of satellite images. *Energy and Buildings*, *169*, 417–429. https://doi.org/10.1016/j.enbuild.2018.03.064

Li, Y., Ding, D., Liu, C., & Wang, C. (2016). A pixel-based approach to estimation of solar energy potential on building roofs. *Energy and Buildings*, *129*, 563–573. https://doi.org/10.1016/j.enbuild.2016.08.025

Lobaccaro, G., & Frontini, F. (2014). Solar Energy in Urban Environment: How Urban Densification Affects Existing Buildings. *Energy Procedia*, *48*, 1559–1569. https://doi.org/10.1016/j.egypro.2014.02.176

Montavon, M. (2010). Optimisation of Urban Form by the Evaluation of the Solar Potential. In *PhD Thesis* (Vol. 4657).

Ouria, M., & Sevinc, H. (2018). Evaluation of the potential of solar energy utilization in Famagusta, Cyprus. *Sustainable Cities and Society*, *37*, 189–202. https://doi.org/10.1016/j.scs.2017.10.036

Perez, R., Ineichen, P., Seals, R., Michalsky, J., & Stewart, R. (1990). Modeling daylight availability and irradiance components from direct and global irradiance. *Solar Energy*, *44*(5), 271–289. https://doi.org/10.1016/0038-092X(90)90055-H

Perez, R., Seals, R., Ineichen, P., Stewart, R., & Menicucci, D. (1987). A new simplified version of the perez diffuse irradiance model for tilted surfaces. *Solar Energy*, *39*(3), 221–231. https://doi.org/10.1016/S0038-092X(87)80031-2

Reinhart, C. F., & Walkenhorst, O. (2001). Validation of dynamic RADIANCE-based daylight simulations for a test office with external blinds. *Energy and Buildings*, *33*(7), 683–697. https://doi.org/10.1016/S0378-7788(01)00058-5

Technology Roadmap: Solar Photovoltaic Energy. (2010). OECD Publishing. https://doi.org/10.1787/9789264088047-en

Wei, L., Tian, W., Silva, E. A., Choudhary, R., Meng, Q., & Yang, S. (2015). Comparative Study on Machine Learning for Urban Building Energy Analysis. *Procedia Engineering*, *121*, 285–292. https://doi.org/10.1016/j.proeng.2015.08.1070

Wiginton, L. K., Nguyen, H. T., & Pearce, J. M. (2010). Quantifying rooftop solar photovoltaic potential for regional renewable energy policy. *Computers, Environment and Urban Systems*, *34*(4), 345–357. https://doi.org/10.1016/j.compenvurbsys.2010.01.001

Wuhan Natural Resources and Planning Bureau. (2011). *Wuhan Urban Master Plan (2010-2020)*. Wuhan Natural Resources and Planning Bureau<http://gtghj.wuhan.gov.cn/pc-69-35849.html>.

Xu, D., Zhou, D., Wang, Y., Meng, X., Chen, W., & Yang, Y. (2020). Temporal and spatial variations of urban climate and derivation of an urban climate map for Xi'an, China. *Sustainable Cities and Society*, *52*, 101850. https://doi.org/10.1016/j.scs.2019.101850

Zhang, J., Zhang, L., Du, M., Zhang, W., Huang, X., Zhang, Y., Yang, Y., Zhang, J., Deng, S., Shen, F., Li, Y., & Xiao, H. (2016). Indentifying the major air pollutants base on factor and cluster analysis, a case study in 74 Chinese cities. *Atmospheric Environment*, *144*, 37–46. https://doi.org/10.1016/j.atmosenv.2016.08.066